Applied Catalysis B: Environmental 96 (2010) 399–407

Contents lists available at ScienceDirect

Applied Catalysis B: Environmental

journal homepage: www.elsevier.com/locate/apcatb

Modeling of a TiO_2-coated quartz wool packed bed photocatalytic reactor

G. Vella [a], G.E. Imoberdorf [b], A. Sclafani [a], A.E. Cassano [b], O.M. Alfano [b,*], L. Rizzuti [a]

[a] Università di Palermo, Dipartimento di Ingegneria Chimica dei Processi e dei Materiali, Unità di Ricerca INCA Palermo 2, Viale delle Scienze, Ed.6 - 90128 Palermo, Italy
[b] INTEC, Instituto de Desarrollo Tecnológico para la Industria Química, Universidad Nacional del Litoral and CONICET, Ruta Nacional N° 168, Km 0, Paraje El Pozo, INTEC I, S3000GLM, Santa Fe, Argentina

ARTICLE INFO

Article history:
Received 12 October 2009
Received in revised form 18 February 2010
Accepted 25 February 2010
Available online 6 March 2010

Keywords:
Packed-bed reactor
Quartz wool
Photocatalysis
TiO_2
Kinetics
Formic acid

ABSTRACT

A fixed-bed, photocatalytic laboratory reactor aimed to degrade pollutants from water streams was designed and built. Quartz wool coated with a thin film of TiO_2 was employed as the reactor filling. The photocatalyst was placed in the reactor forming a loose packing to guarantee the intimate contact among reactants, photons, and the photocatalytic surface. This reactor was employed to study the photocatalytic decomposition of a model pollutant (formic acid). A reactor–radiation–reaction model was developed, which was comprised of the reactor mass balance, radiation model, and kinetic model for the degradation of formic acid. The local superficial rate of photon absorption, which was necessary to evaluate the kinetic, was obtained from the results of a radiation model. The Monte Carlo approach was employed to solve the radiation model, where the interaction between photons and the TiO_2-coated fibers of the packing was considered. The kinetic model was derived from a plausible kinetic scheme. Experimental results obtained in the packed-bed reactor, operating in a differential mode and without mass transfer limitations, were used to estimate the parameters of the kinetic model. A satisfactory agreement was observed between model simulations with the derived parameters and experimental results, with a root mean square error less than 8.3%.

1. Introduction

In a previous work [1], a radiation model for the TiO_2-coated quartz wool packed bed photocatalytic reactor was presented. In this publication, this radiation model was coupled with the corresponding mass balances and a kinetic model to describe a packed-bed photocatalytic reactor applied for the degradation of formic acid (FA). This research is closely connected to three important areas of photocatalysis: modeling of packed-bed photocatalytic reactors, the implementation of the Monte Carlo method to solve the radiative transfer equation (RTE) in complex geometries, and the use of a model pollutant for kinetic modeling purposes.

Concerning exclusively to packed-bed photocatalytic reactors, the first contribution goes back to 1988 and was made by Al-Ekabi and Serpone [2], who built a photocatalytic reactor filled with a glass matrix coated with TiO_2. A few years later, Sclafani et al. [3] reported a packed-bed reactor made of small spheres of pure TiO_2. The authors obtained high photocatalytic reaction rates but, at the same time, unmistakable mass transfer limitations. Crittenden et al. [4] used TiO_2 small particles in a packed-bed reactor to treat water polluted with chlorinated hydrocarbons. Changrani and Raupp [5,6] made a significant theoretical contribution, since they proposed a complete model to describe a reticulated-foam packed-bed reactor. Vorontsov et al. [7] employed a packed-bed of very small particles of TiO_2 placed at the bottom of a photocatalytic reactor for pollutant degradation studies. Dionysiou et al. [8] developed a rotating disk, packed-bed, photocatalytic reactor for the decontamination of a mixture of contaminants and analyzed the role of mass transfer during the process. Finally, Ibhadon et al. [9] used a custom-made TiO_2-coated foam reactor to investigate the degradation of volatile organic compounds in gaseous phase.

Subsequent to the pioneering proposal of Spadoni et al. [10], the Monte Carlo approach was used to estimate the radiation distribution for different types of photoreactors. Yokota et al. [11] proposed a pseudo-homogeneous approach for evaluating the radiation propagation in a suspension of small particles; Pasquali et al. [12], Yokota et al. [13], and Yang et al. [14] modeled the radiation field inside slurry photocatalytic reactors taking into account the radiation absorption and scattering of titanium dioxide; Imoberdorf et al. [15] investigated the interaction between UV radiation and TiO_2-coated spheres; Brucato et al. [16] used MC simulations to validate the Six Flux Model, to solve the RTE and to improve the radiation field uniformity in a photoreactor [17]; and Alexiadis [18] and Singh et al. [19] studied the radiation distribution in photocatalytic monolith reactors for air treatment.

* Corresponding author. Tel.: +54 0342 4511370/72/73/74x1056; fax: +54 0342 4511087.
E-mail addresses: alfano@intec.unl.edu.ar.ar, alfano@ceride.gov.ar (O.M. Alfano).

0926-3373/$ – see front matter © 2010 Elsevier B.V. All rights reserved.
doi:10.1016/j.apcatb.2010.02.037

Nomenclature

A	surface (cm^2)
C	concentration (mg/L)
$e^{a,S}$	local surface rate of photon absorption ($Eins\,s^{-1}\,m^{-2}$)
O.F.	objective function, dimensionless
G	incident radiation ($mW\,cm^{-2}\,sr^{-1}$)
I	radiation specific intensity ($mW\,cm^{-2}$)
k	kinetic parameter, units depend on the particular reaction involved
K_{FA}	adsorption equilibrium constant of FA ($L\,mg^{-1}$)
M	mass (mg)
MFP	mean free path (cm)
n	number of photons or lamps
$\underline{n}$	vector normal to a given surface
P_{lamp}	effective emission power of the lamp (W)
q	local net radiation flux ($mW\,cm^{-2}$)
Q	volumetric flow rate (cm^3/min)
R	radius (cm)
r_g	electrons and holes generation rate ($mol\,cm^{-2}\,s^{-1}$)
t	average TiO_2 film thickness (μm)
T	transmittance (%)
V	volume (cm^3)
x	rectangular coordinate (cm)
y	rectangular coordinate (cm)
z	rectangular coordinate (cm)

Greek symbols

κ	volumetric absorption coefficient (cm^{-1})
θ	polar angle (rad)
ρ	density ($g\,cm^{-3}$)
ϕ	azimuthal angle (rad)
Φ	primary quantum yield ($mol\,Eins^{-1}$)
Ω	solid angle (sr)
$\underline{\Omega}$	unit vector in the direction of propagation of a beam

Subscripts

ads	relative to adsorbed species
FA	relative to the formic acid
feed	relative to the feed
fiber	relative to the quartz fibers
in	relative to the inlet
lamp	relative to the lamp
loc	local value
out	relative to the outlet
quartz	relative to the quartz of the fibers
R	relative to the reactor
A	relative to the area
TiO_2	relative to the TiO_2 films
V	relative to the volume
λ	denotes wavelength

Superscripts

exp	refer to the experimental values
i	refer to the radiation incident on a given surface
in	refer to the recycle system inlet
inlet	refer to the reactor inlet
mod	refer to the modeling values
out	refer to the recycle system outlet
outlet	refer to the reactor outlet

Special symbols

$\langle\cdot\rangle$	means average value over a given interval
$\underline{\ }$	denotes a vector in the three-dimensional space

Regarding the pollutant employed in this study, FA has been used as model compound in several areas of advanced oxidation technologies, such as H_2O_2/UV, photo-Fenton reactions, and photocatalysis due to its absence of stable by-products, high solubility in water, and low vapor pressure (to avoid undesirable air stripping). Specifically in the field of photocatalysis, Kim and Anderson [20] studied the degradation of FA in a porous TiO_2 thin-film electrode and analyzed the use of these devices in electrophotocatalytic systems. Kesselman et al. [21] compared hydroxyl radical and direct hole oxidation mechanisms by studying the degradation of FA in a polycrystalline Nb-doped TiO_2 electrode. Candal et al. [22] analyzed the effect of pH and the applied potential on the photocurrent and the oxidation rate of saline solutions of FA in a photo-electrolytic reactor using TiO_2 electrodes. A significant contribution concerning catalyst immobilization was made by Dijkstra et al. [23], who proposed a complete reaction scheme for the photocatalytic decomposition of FA. McMurray et al. [24] studied the intrinsic kinetics of the decomposition of oxalic and formic acids using immobilized Degussa P-25 TiO_2 films. Krýsa et al. [25] studied the degradation of FA and other organic compounds (oxalic acid, 4-chlorophenol and the herbicide 3-(4-chlorophenyl)-1,1-dimethylurea) using particulate films of TiO_2. The authors concentrated their efforts in modeling the reaction kinetics and analyzing the role of competitive adsorption of the organic compounds. Finally, and without the intention of being totally exhaustive, one can mention the work of Mrowetz and Selli [26], who studied the photocatalytic degradation of FA and benzoic acid in water suspensions using TiO_2 and ZnO as photocatalysts. The authors interpreted their results in terms of a pseudo-steady-state Langmuir–Hinshelwood rate kinetics and reported the dependence of the reaction rate on the reaction pH

This work is aimed at the proposal of a reactor–radiation–reaction model for describing the rate of FA degradation (chosen as a model pollutant) in a packed-bed photocatalytic reactor filled with TiO_2-coated glass wool. Computer simulations were used to obtain the kinetic parameters by comparing model predictions with the experimental results obtained in the laboratory reactor

2. Experimental

2.1. Experimental set-up and operating conditions

Experiments were carried out in a thin, flat plate, packed-bed reactor that was loosely filled with a quartz wool coated with TiO_2 [1]. This configuration guaranteed a good contact between the solution with the aqueous pollutant, the photons emitted by the UV lamps, and the TiO_2 catalytic surface. The reactor is shown in Fig. 1 and the lamps and reactor characteristics are summarized in Table 1. Both sides of the reactor, made of borosilicate glass, were irradiated with two tubular UV-fluorescent lamps (Philips BL TL-K 40W/10-R). The lamps were arranged in such a way that allowed the regulation of their distance to the reactor windows, in order to change the reactor irradiation level. The lamps have an emission spectrum ranging from 340 to 420 nm, with a peak at 370 nm ([1], Fig. 2(a)). Most of the emission power of the lamp is in the range between 400 and 340 nm. Reactor windows were kept in a parallel position by two polymethylmetacrilate heads, in which inlet and outlet fluid distributors were located. The set-up had provisions

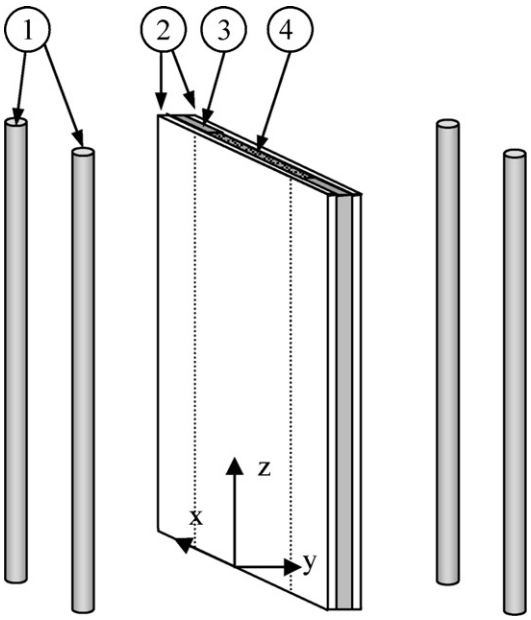

Fig. 1. Geometry of the photocatalytic reactor: (1) UV lamps, (2) borosilicate glass windows, (3) aluminum rod with rubber seal gaskets, (4) TiO_2-coated quartz wool.

Table 1
Lamp and reactor descriptions.

Item	Values
Lamp type	Philips BL-K 40W/10-R
Lamp power	P_{lamp} = 6.8 W
Lamp dimensions	Z_{lamp} = 60 cm, R_{lamp} = 1.3 cm
Reactor width	$X_{reactor}$ = 9.6 cm
Reactor thickness	$Y_{reactor}$ = 0.5 cm
Reactor length	$Z_{reactor}$ = 50 cm
Reactor windows	Made of borosilicate glass
Reactor packing	17.2 g quartz wool with 14.4% w/w TiO_2

for recycling the reacting solution in a closed loop by means of a peristaltic pump (Fig. 2).

The feed, previously prepared with distilled water and FA at different concentrations, was placed in a tank, and pumped by means of a peristaltic pump (CELLAI 503 U) into the recycle flow tubing, just before the packed-bed reactor inlet.

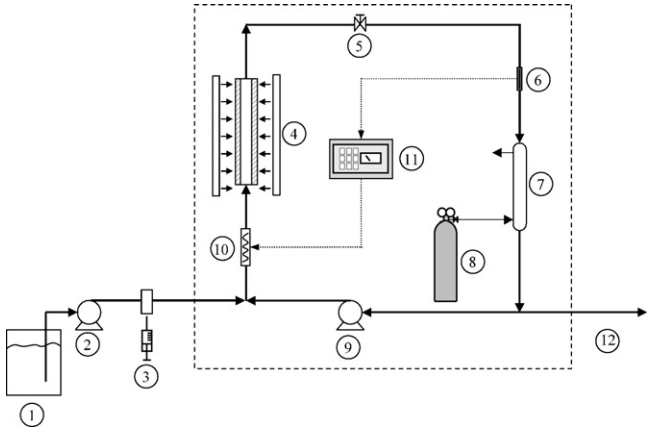

Fig. 2. Flow sheet of the experimental device: (1) feed tank, (2) feed pump, (3) sampling point at recycle inlet ($C_{FA}^{in}\big|_{recycle}$), (4) photocatalytic reactor with UV lamps, (5) sample valve, (6) thermocouple, (7) packed column, (8) O_2 cylinder, (9) recycle pump, (10) resistor, (11) temperature controller, and (12) liquid outlet ($C_{FA}^{out}\big|_{recycle}$).

A packed column was used to treat the reacting solution in counter current mode with a pure oxygen gaseous stream. The objective of this column was: (i) to saturate the reacting solution with oxygen in order to avoid any complication arising by oxygen deficiency in the reacting system and (ii) to strip CO_2, which was produced by the mineralization of the organic substrate. The oxygen saturation was checked by means of a WTW CellOx325 electrode sensor and a WTW Oxi 340i control unit. The liquid hold-up of the entire set-up was about 600 mL.

The experimental set-up permitted operating of the whole system under steady state conditions, handling the photocatalytic reactor under differential conversions, and, with proper control of the flow and irradiation rates, avoiding any form of mass transfer limitations. A thermocouple connected by means of a PID temperature controller to a resistor wire was used to guarantee an isothermal operation of the system.

2.2. Catalyst preparation

The TiO_2 was immobilized on the quartz wool surface using the sol–gel technique [27]. A first solution was prepared mixing a volume of 20 mL of Ti(IV) isopropoxide with 500 mL of isopropyl alcohol, and then 520 mL of the same solvent was added. Separately, a second solution was prepared with 91 mL of isopropyl alcohol and 520 mL of an acid solution of bidistilled water and of HCl (pH 1). These two solutions were mixed together to obtain a whitish sol with small particles of TiO_2. To wash the support, 17.2 gr of quartz wool were soaked with an aqueous solution of HCl (pH 3) during 3 h and then dried in an oven at 55 °C for 12 h. The pretreated quartz wool was fully immersed in the TiO_2 sol in order to become entirely impregnated with the catalyst. Afterwards, the resulting coated support was drained and dried in an oven at 55 °C during 22 h to remove the residual volatile organics. Then, it was maintained in the oven at 250 °C for 3 h to remove of any form of chlorinated residuals that could had been formed. This procedure, starting from the impregnation step, was repeated four times in order to improve the mechanical stability and adherence of the TiO_2 film to the quartz support. Finally, to ensure the formation of anatase, the coated packing was calcined during 4 h in a furnace at 400 °C. The immobilization procedure was completed after washing several times the coated packing with bidistilled water. The average value of the obtained catalyst supported mass was 144 mg of TiO_2 per gram of bed. XRD measurements showed that all the immobilized TiO_2 was in the anatase form.

Once the preparation was completed, the TiO_2-coated quartz wool was housed inside the reactor, and additional washings were performed to remove loosely adhered TiO_2 to the glass wool. This washing procedure was repeated until spectrophotometric measurements revealed that no TiO_2 was present in the residual water.

2.3. Experimental procedures

Experimental runs were carried out by varying the following three parameters: (i) the initial concentration of the contaminant (FA), (ii) the radiation flux reaching the reactor windows, and (iii) the feed flow rate. Details of the operating conditions are summarized in Table 2.

For each experimental run, the system was filled up with the solution to be treated, the recycle pump and the temperature control system were switched on to reach the fluid-dynamic and thermal steady state. In the mean time, oxygen was fed to the packed column, and the lamps were switched on in order to stabilize the photon emission, which was achieved in about 30 min. During this time, the lamps were shielded to prevent radiation from reaching the photocatalytic reactor. Temperature, oxygen concentration, and irradiation level were measured to check that constant

Table 2
Operating conditions.

Item	Values
Operating temperature	35 °C
Inlet and outlet flow rate	5–20 cm^3/min
Recycle flow rate	480 cm^3/min
Inlet FA concentration	50–500 mg/L
Radiation flux	0.77–3.5 mW cm^{-2}

values were reached, i.e., that the system had attained steady state operation. At this point, the feed pump was turned on, the lamps were unshielded, and sampling began. Water samples were taken during the course of the treatment until constant values of the outlet FA concentration were obtained, indicating that the whole system has reached steady state. Typically, each run ended after 4–5 h.

Samples were analyzed using HPLC (column Alltech Waters Spherisorb® C8, 5 μm, 250 mm × 4.8 mm, with UV detector) for FA concentrations larger than 100–200 mg/L, while ion chromatography (Metrohm, Anion dual 1.3 mm × 150 mm) was preferred for lower FA concentrations.

To test the stability of the photocatalyst, a control test was performed under specific operating conditions just at the beginning of the experimental study and after 5 months of operation, and the same experimental results were obtained, proving that no deactivation took place.

3. Mass balance for the differential fixed-bed reactor

The numerical values of the FA degradation rate were obtained from experimental results by applying a mass balance to the recycle system (dashed lines in Fig. 2):

$$\int_{A_R} r_{FA}(\underline{x})\ \mathrm{d}A_R = Q_{Feed}\left(C_{FA}^{out}\big|_{recycle} - C_{FA}^{in}\big|_{recycle}\right) \quad (1)$$

where $r_{FA}(\underline{x})$ is the FA surface degradation rate, A_R is the photocatalytic area of the reactor, Q_{Feed} is the volumetric flow rate of the recycling system feed, and $C_{FA}^{in}|_{recycle}$ and $C_{FA}^{out}|_{recycle}$ are the FA concentrations at the inlet and outlet of the recycle, respectively. It should be noted that $r_{FA}(\underline{x})$ is a function of the local concentration of the reactants on the surface of the photocatalyst and of the local rate of photon absorption on the same surface:

$$r_{FA}(\underline{x}) = f[C_{FA,loc}(\underline{x}), e^{a,S}(\underline{x})] \quad (2)$$

where $e^{a,S}$ is the local surface rate of photon absorption (LSRPA) [28]. The reactor recycle inlet and outlet concentrations were measured in all cases after the reactor reached the steady state. For all the experimental runs, the value of the recycle flow rate was relatively high (480 cm^3/min) in comparison with the employed inlet flow rates (5–20 cm^3/min). Under the adopted operating conditions, it can be shown that FA concentrations at the reactor inlet and outlet were very similar, and their respective values differed by less than 3.6%, proving that the differential reactor assumption is acceptable:

$$\frac{\left(C_{FA}^{in}\big|_{reactor} - C_{FA}^{out}\big|_{reactor}\right)}{C_{FA}^{in}\big|_{reactor}} \times 100 \le 3.6\% \quad (3)$$

In addition, the recirculation flow rate was large enough to reduce diffusive resistances to negligible levels. Some experimental runs were performed at different recycling flow rates to check the absence of mass diffusion controlling phenomena. No significant differences were found between these runs, thus confirming that mass transport restrictions did not play any important role in the process.

By taking into account both the differential reactor operation and the kinetic controlling regime assumptions, the concentration of FA can be considered to be uniform in all the reactor volume and equal to the recycle outlet concentration:

$$C_{FA}(\underline{x})\big|_{reactor} \cong C_{FA}^{out}\big|_{recycle} \quad (4)$$

Regarding the radiation flux, the rate of photon absorption has small variations along the x and z coordinates, but presented a significant dependence on the y coordinate [1].

4. Reaction scheme of formic acid photocatalytic degradation

Based on the plausible reaction schemes proposed by Dijkstra et al. [23] and by Krýsa et al. [25], a kinetic expression was derived. Table 3 shows the steps involved in the reaction scheme adopted. In broad terms, photocatalytic processes are based on the action of highly oxidative, short lived, intermediate compounds that are generated when a TiO_2 is activated by UV radiation. Photocatalytic reactions begin with the generation of electron–hole pairs in the irradiated TiO_2 bulk (Table 3, reaction (0)). To prevent the recombination of the charge carriers, electrons and holes have to be trapped. Holes may react with adsorbed water and surface OH^- ions to generate $^\bullet OH$ radicals (reaction (1)), whereas electrons can be trapped by oxygen, generating superoxide radicals (reaction (2)). The presence of oxygen on the photocatalyst surface is very important to prevent the reduction of the Ti^{4+} to Ti^{3+}, which would produce a drastic decrease of the photocatalytic activity of TiO_2. The electrons and holes that are not trapped can recombine, and energy will be lost as heat (reaction (10)).

The FA photocatalytic degradation in aqueous phase, according to independent studies conducted by Kesselman et al. [21], McMurray et al. [24] and Krýsa et al. [25] may be produced by two parallel steps: (i) reaction attack by $^\bullet OH$ radicals (reaction (3)) and (ii) direct attack by the photogenerated holes (reaction (4)). This subject is still controversial and the preponderance of one or the other attack seems to be associated with the working pH, the characteristics of the adsorbed pollutant on the catalytic surface, and the behavior of the employed catalyst. Wolf et al. [29] and Bahnemann et al. [30] supported the second mechanism particularly for those cases where the organic compound can be strongly adsorbed on the catalytic surface. However, the majority of the photocatalytic reports on photocatalytic oxidation advocated the first mechanism, arguing that $^\bullet OH$ radicals have very high oxidizing properties.

In obtaining the kinetic expression from the proposed scheme, the following assumptions were made:

1. The degradation of FA only takes place on the surface of the irradiated photocatalyst, and no photolytic degradation occur when

Table 3
Formic acid photocatalytic degradation scheme [23,25].

Reaction	Reaction steps	Reaction rates
0	$TiO_2 + h\upsilon \rightarrow TiO_2 + e^- + h^+$	r_g
1	$h^+ + H_2O_{ads} \rightarrow {}^\bullet OH + H^+$ $h^+ + HO^-_{ads} \rightarrow {}^\bullet OH$	$k_1\,[H_2O]_{ads}\,[h^+]$
2	$e^- + O_{2,ads} \rightarrow {}^\bullet O_2^-$	$k_2\,[O_2]_{ads}\,[e^-]$
3	$HCOOH_{ads} + {}^\bullet OH \rightarrow HCOO^\bullet + H_2O$	$k_3\,[FA]_{ads}\,[{}^\bullet OH]$
4	$HCOOH_{ads} + h^+ \rightarrow HCOO^\bullet + H^+$	$k_4\,[FA]_{ads}\,[h^+]$
5	$HCOO^\bullet + O_{2,ads} \rightarrow CO_2 + H^+ + {}^\bullet O_2^-$	$k_5\,[HCOO^\bullet]_{ads}\,[O_2]_{ads}$
6	$^\bullet OH + H^+ \rightarrow h^+ + H_2O_{ads}$	$k_6\,[{}^\bullet OH]\,[H^+]$
7	$^\bullet OH + OH^- \rightarrow O^{\bullet -} + H_2O_{ads}$	$k_7\,[{}^\bullet OH]\,[OH^-]$
8	$2HO_2^\bullet \rightarrow H_2O_{2,ads} + O_2$	$k_8\,[HO_2^\bullet]^2$
9	$H_2O_{2,ads} + {}^\bullet OH \rightarrow H_2O + HO_2^\bullet$	$k_9\,[H_2O_2]_{ads}\,[{}^\bullet OH]$
10	$e^- + h^+ \rightarrow$ heat	$k_{10}\,[e^-][h^+]$
11	$2{}^\bullet OH \rightarrow H_2O_{2,ads}$	$k_{11}\,[{}^\bullet OH]^2$

the reactor is irradiated in the absence of TiO_2. This assumption can be justified taking into account that FA does not absorb UV radiation in the wavelength range of the employed lamps (340–420 nm).

2. Since radical species are very reactive, the rate of generation of radicals can be considered equal to their rate of disappearance. Therefore, the kinetic micro-steady-state approximation (MSSA) for radical intermediates applies.
3. FA degradation is mostly driven by the •OH radical attack: •OH radicals are highly oxidizing and reactive; consequently they are able to capture easily electrons from organic compounds causing their oxidation. In the current work, we assume that the attack by •OH radicals is faster than the direct attack by the photogenerated holes:

$$k_4[\mathrm{FA}]_{ads}[h^+] \ll k_3[\mathrm{FA}]_{ads}[\cdot\mathrm{OH}] \quad (5)$$

4. This leads to the conclusion that the consumption rate of photogenerated holes by FA direct attack can be neglected when compared with those corresponding to reactions (1) and (10) in Table 3:

$$k_4[\mathrm{FA}]_{ads}[h^+] \ll k_1[H_2O]_{ads}[h^+] + k_{10}[e^-][h^+] \quad (6)$$

The value of k_3 and k_{11} are 1.3×10^8 and $4\times10^9\ \mathrm{mol\,L^{-1}\,s^{-1}}$, respectively [31]. Even when the order of magnitude of k_3 is lower to that of k_{11}, the expected order of magnitude of the concentration of •OH is much lower than that of FA. Therefore, the second-order radical reaction between •OH radicals (reaction 11 in Table 3) is neglected in the •OH radicals balance when compared with the rate of FA degradation (reaction 3):

$$k_3[\mathrm{FA}]_{ads}[\cdot\mathrm{OH}] \gg k_{11}[\cdot\mathrm{OH}]^2 \quad (7)$$

Based on these considerations, as it is shown in Appendix I, the following local value of the reaction rate is obtained:

$$r_{FA} = -\frac{K_1 C_{FA}}{1+K_2 C_{FA}}\left(\sqrt{1+K_3 e^{a,S}}-1\right) \quad (8)$$

The average value of the FA degradation rate on the photocatalytic surface of the reactor is:

$$\langle r_{FA}\rangle_{A_R} = \frac{\int_{A_R} r_{FA}(\underline{x})\,dA_R}{A_R} \quad (9)$$

Substituting Eq. (8) into Eq. (9):

$$\langle r_{FA}\rangle_{A_R} = -\frac{1}{A_R}\int_{A_R}\frac{K_1 C_{FA}(\underline{x})}{1+K_2 C_{FA}(\underline{x})}\left(\sqrt{1+K_3 e^{a,S}(\underline{x})}-1\right)dA_R \quad (10)$$

The concentration of FA was uniform in the reactor volume because the reactor operated under differential mode and kinetic controlling regime. However, as mentioned, the LSRPA varied with the y coordinate of the reactor. By applying Eq. (10) to the reacting system, we obtain:

$$\langle r_{FA}\rangle_{A_R} = -K_1\frac{C_{FA}^{out}\big|_{recycle}}{1+K_2\,C_{FA}^{out}\big|_{recycle}}\frac{\int_{A_R}\left(\sqrt{1+K_3 e^{a,S}(\underline{x})}-1\right)dA_R}{A_R} \quad (11)$$

5. Radiation model

Prior to the presentation of the radiation model, the optical properties and radiative variables are defined. The spectral incident radiation is defined as [32]:

$$G_\lambda(\underline{x}) = \int_\Omega I_\lambda(\underline{x},\underline{\Omega})\,d\Omega = \int_{\theta=0}^{\pi/2}\int_{\phi=0}^{2\pi} I_\lambda(x,y,z,\phi,\theta)\sin\theta\,d\phi\,d\theta \quad (12)$$

The local net spectral radiation flux is:

$$q_\lambda(\underline{x}) = \int_\Omega I_\lambda(\underline{x},\underline{\Omega})\underline{\Omega}\cdot\underline{n}\,d\Omega = \int_{\theta=0}^{\pi/2}\int_{\phi=0}^{2\pi} I_\lambda(x,y,z,\phi,\theta)\ \sin\theta\cos\theta\,d\phi\,d\theta \quad (13)$$

where $I_\lambda(\underline{x},\underline{\Omega})$ is the spectral radiation intensity associated with the energy of the beams reaching a given surface at the point $\underline{x}$, whose direction is defined by the unit vector $\underline{\Omega}=\underline{\Omega}(\theta,\phi,1)$, $\underline{n}$ is the upwardly directed unit vector normal to the photocatalytic surface, and $d\Omega=\sin\theta\ d\phi\ d\theta$ is the differential solid angle around the direction of propagation $\underline{\Omega}$.

The local net radiation flux considers the complete wavelength range of the radiation that is absorbed by the catalyst:

$$q(\underline{x}) = \sum_{\lambda_{min}}^{\lambda_{max}} q_\lambda(\underline{x}) \quad (14)$$

The local surface rate of photon absorption (LSRPA or $e^{a,S}$) is defined as:

$$e^{a,S}(\underline{x}) = \sum_{\lambda_{min}}^{\lambda_{max}}\int_{t=0}^{t_{TiO_2}}\kappa_\lambda(\underline{x})G_\lambda(\underline{x})\,dt = q^i(\underline{x}) - q^t(\underline{x}) \quad (15)$$

where $\kappa_\lambda(\underline{x})$ is the spectral volumetric absorption coefficient of pure TiO_2, $q^i(\underline{x})$ and $q^t(\underline{x})$ are the local net radiation fluxes incident on the TiO_2 film and transmitted through it, respectively, and t_{TiO_2} is the thickness of the TiO_2 films.

As mentioned, from the kinetic viewpoint, it is necessary to evaluate the surface photon absorption rate ($e^{a,S}$) in the TiO_2 films by using a radiation model because it cannot be measured experimentally without disturbing the existing radiation field. Consequently, the $e^{a,S}$ in the TiO_2 films was evaluated using a radiation model.

In a previous publication [1], a Monte Carlo, photocatalytic packed-bed radiation model (MCPPR model) was presented. In a brief summary, the model considers the following events:

- In order to consider the particularities of the employed lamps, photons are considered to be isotropically emitted by half of the lamp surface [Fig. 3(1)].

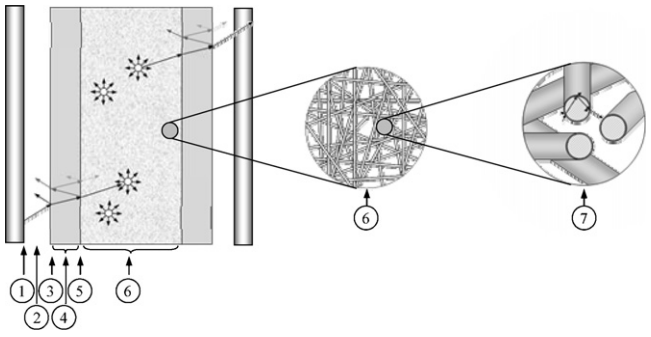

Fig. 3. Schematic representation of the photocatalytic reactor and the events considered in the radiation model: (1) lamps surface, (2) air between lamps and the reactor, (3) air–glass interface, (4) borosilicate glass windows, (5) glass–water interface, (6) reactor filling (aqueous phase and photocatalytic bed), (7) detailed scheme of the TiO_2-coated fibers.

- When traveling in the air phase between the lamps and the reactor windows, photons follow a linear trajectory, neither being absorbed nor scattered, since air is a non-participative medium [Fig. 3(2)].
- Those photons that reach the air–glass interface at the reactor wall entrance, can be reflected or transmitted [Fig. 3(3)].
- When traveling in the reactor windows, photons follow a linear trajectory, but are partially absorbed in the borosilicate glass. The possibility of internal multi-reflection inside the wall is considered by the model [Fig. 3(4)].
- Those photons that reach the glass–water interface at the reactor wall entrance can be reflected or transmitted [Fig. 3(5)].
- When traveling in the reactor water-bed system [Fig. 3(6)], photons may interact with the TiO_2-coated fibers, following a series of coupled events. Photons travel with a linear trajectory in the aqueous phase until they reach a TiO_2-coated fiber, the reactor windows, or the reactor walls. Those photons that reach the fibers, can be absorbed by the TiO_2 films, reflected on the surface, or transmitted. The possibility of internal multi-reflection in the quartz fibers is also considered by the model [Fig. 3(7)]. Photons traveling inside the quartz fibers are not absorbed, because the spectral volumetric absorption coefficient of quartz in the wavelength range emitted by the lamps is negligible. Those photons that are transmitted by the fibers towards the aqueous phase may interact with other fibers, until they are absorbed or reach the reactor windows or walls.
- Those photons at the air–glass interface whose direction implies to go away from the reactor (i.e., photons that abandon the reactor) are considered lost and a new photon is considered.
- The absorption location of those photons that are absorbed in the TiO_2 film is stored and a new photon is considered.
- Those photons that are absorbed in the borosilicate glass walls are considered lost and a new photon is considered.

The mentioned series of events was modeled by considering the following assumptions:

(1) Photons were emitted individually, where their emission point on the lamp surface, propagation direction, and wavelength were stochastically defined considering the particularities of the employed lamps.
(2) Photon tracking was based on laws of geometric optics.
(3) Those photons that reach the reactor windows can be reflected or refracted. The angle-dependant local reflectivity was calculated using the Fresnel equation [33].
(4) The propagation direction of reflected photons was determined considering specular reflection, whereas the propagation direction of the refracted photons was evaluated using the Snell law [33].
(5) The photocatalyst consisted of a great number of TiO_2-coated quartz fibers, which were uniformly distributed inside the reactor. The axis of each fiber was assumed parallel to the reactor windows and its angle with respect to the z coordinate was randomly assigned.
(6) The mean free path of photons inside the reactor was estimated as the volume of the reactor divided by the total sum of the projected area of the fibers:

$$\mathrm{MFP} = \frac{V_R}{A^{\mathrm{long}}_{\mathrm{fiber,T}}} \tag{16}$$

where MFP is the mean free path and $A^{\mathrm{long}}_{\mathrm{fiber,T}}$ is the total sum of the projected area of the fibers (it was estimated from micrographic determinations of the quartz wool).

(7) Plausible photon advances inside the reactor were estimated by:

$$\xi = -\mathrm{MFP}\ \mathrm{Ln}(R) \tag{17}$$

where R is an uniformly distributed random number.

(8) The spectral volumetric absorption coefficient of the TiO_2 was calculated by using the correlation proposed by Sodergren et al. [34]:

$$\kappa_\lambda = \exp 29 - 85\lambda \tag{18}$$

where κ_λ is the spectral volumetric absorption coefficient of the TiO_2 in μm^{-1}, and λ is the wavelength in μm.

(9) The effective transmittance of the TiO_2 films was evaluated by considering the spectral volumetric absorption coefficient of pure TiO_2 and the average thickness of the films:

$$T_{\mathrm{film\ TiO_2}} = \exp(-\kappa_\lambda t_{\mathrm{TiO_2}}) \times 100 \tag{19}$$

(10) The average thickness of the TiO_2 films was estimated by considering that all the TiO_2 was uniformly distributed on the total available surface of the quartz wool fibers. The numerical value was calculated by considering the total mass of the filling and the density of TiO_2 immobilized on the photocatalyst, the mass and the density of the fibers, and their diameter distribution [1]:

$$t_{\mathrm{k,TiO_2}} = \frac{M_{\mathrm{TiO_2}}\rho_{\mathrm{quartz}}}{2M_{\mathrm{fiber}}\rho_{\mathrm{TiO_2}}} \frac{\sum_{R=R_{\min}}^{R_{\max}} n_R R^2_{\mathrm{fiber}}}{\sum_{R=R_{\min}}^{R_{\max}} n_R R_{\mathrm{fiber}}} \tag{20}$$

The resulting value was: $t_{\mathrm{k,TiO_2}} = 0.687\ \mu m$. The size distribution of fiber radii was estimated from micrographic determinations performed in the quartz wool.

An ad hoc program to compute the trajectory of photons was developed. The absorption place of photons in the TiO_2 films was stored in a matrix that corresponds to the discretized reactor volume. This matrix, with the information of the absorption position of all photons, was used to calculate the $e^{a,S}$ in the reactor:

$$e^{a,S}(x,y,z) = n_{\mathrm{ph,absorbed}}(x,y,z) \frac{n_{\mathrm{lamp}} P_{\mathrm{lamp}}}{n_{\mathrm{ph,T}} \Delta x \Delta y \Delta z} \frac{V_R}{A_R} \tag{21}$$

where $n_{\mathrm{ph,absorbed}}(x,y,z)$ is the number of photons absorbed in the element corresponding to the coordinates (x,y,z), n_{lamp} is the number of lamps, P_{lamp} is the emission power of each lamp, $n_{\mathrm{ph,T}}$ is the total number of photons considered in the model, and $\Delta x \Delta y \Delta z$ is the volume of each element. The previous procedure was repeated to calculate the absorption radiation distribution for each radiation level used in the experimental runs. The results are shown in Fig. 4(a) and (b).

6. Experimental results and estimation of kinetic parameters

The parameters in the kinetic expression (K_1, K_2 and K_3) were regressed from experimental data using the Levenberg–Marquardt method. The FA reaction rate (Eq. (11)) was computed using the corresponding FA concentration at the outlet stream of the loop. The predicted values of the outlet FA concentrations were obtained substituting the kinetic expression [Eq. (11)] into the mass balance applied to the recycle system (Eq. (1)):

$$Q_{\mathrm{Feed}} \left(C^{\mathrm{out}}_{\mathrm{FA}}\big|_{\mathrm{recycle}} - C^{\mathrm{in}}_{\mathrm{FA}}\big|_{\mathrm{recycle}} \right) = -K_1 \frac{C^{\mathrm{out}}_{\mathrm{FA}}\big|_{\mathrm{recycle}}}{1 + K_2\, C^{\mathrm{out}}_{\mathrm{FA}}\big|_{\mathrm{recycle}}} \int_{A_R} \left(\sqrt{1 + K_3 e^{a,S}} - 1 \right) \mathrm{d}A_R \tag{22}$$

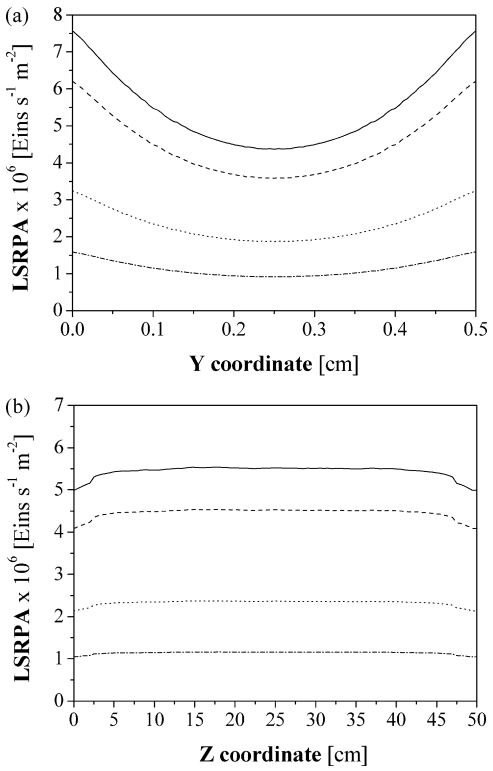

Fig. 4. (a) Transversal and (b) longitudinal LSRPA profiles inside the reactor when the lamps are located at 4.5 (—), 7.5 (—), 15 (···), and 30 (-·-·) cm from the reactor.

And finally, the outlet FA concentration can be obtained from Eq. (22):

$$C_{FA}^{out}\Big|_{recycle}^{mod} = \frac{C_{FA}^{in}K_2Q_{Feed} - K_1\int_{A_F}\left(\sqrt{1+K_3e^{a,S}}-1\right)\,dA_F - Q_{Feed}}{2K_2Q_{Feed}} + \frac{\sqrt{4C_{FA}^{in}K_2Q_{Feed}^2 + \left(C_{FA}^{in}K_2Q_{Feed} - K_1\int_{A_F}\left(\sqrt{1+K_3e^{a,S}}-1\right)\,dA_F - Q_{Feed}\right)^2}}{2K_2Q_{Feed}} \quad (23)$$

Since the kinetic expression is coupled with the radiation field, the values of the radiation absorption rates ($e^{a,S}$) obtained using the radiation model were used to solve Eq. (23).

The optimizing program minimized the sum of the square of the relative differences between predicted and experimental values of the outlet FA concentration (objective function):

$$O.F. = \sum_{i=1}^{n_{data}}\left(\frac{C_{FA}^{out}\Big|_{recycle}^{exp} - C_{FA}^{out}\Big|_{recycle}^{mod}}{C_{FA}^{out}\Big|_{recycle}^{exp}}\right)^2 \quad (24)$$

After analyzing the values of the kinetic parameters that best fit experimental results, it was concluded that:

$$K_3e^{a,S} \ll 1 \quad (25)$$

Thus, from the mathematical point of view, the kinetic model can be simplified after expanding Eq. (11) using the Taylor expansion [35]:

$$\langle r_{FA}\rangle_{A_R} = -K_1^*\frac{C_{FA}^{out}\Big|_{recycle}\langle e^{a,S}(\underline{x})\rangle_{A_R}}{1+K_2\,C_{FA}^{out}\Big|_{recycle}} \quad (26)$$

where

$$K_1^* = \frac{K_1K_3}{2} = \frac{k_3K_{FA}[sites]}{k_s}\langle\Phi\rangle \quad (27)$$

Table 4
Kinetic parameters.

Parameter	Value	95% confidence interval	Units
K_1^*	0.054	0.015	$m^3\ Eins^{-1}$
K_2	7.126	0.058	$m^3\ kg^{-1}$

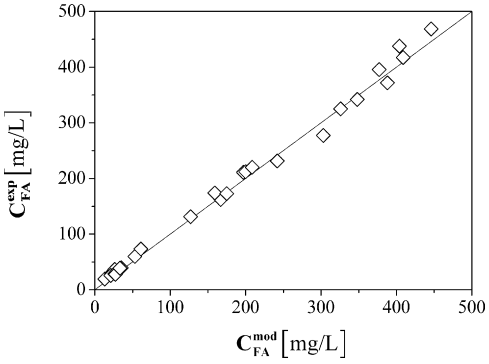

Fig. 5. Experimental against predicted values of FA output concentrations for different operating conditions.

Eq. (26) presents a similar functionality than the Langmuir–Hinshelwood kinetics, but the meaning of the involved kinetic constants is different (Eqs. (A-13) and (27)).

From Eqs. (26) and (1), we obtain:

$$C_{FA}^{out}\Big|_{recycle}^{mod} = \frac{C_{FA}^{in}K_2Q_{Feed} - K_1^*\langle e^{a,S}(\underline{x})\rangle_{A_R}A_F - Q_{Feed}}{2K_2Q_{Feed}} + \frac{\sqrt{4C_{FA}^{in}K_2Q_{Feed}^2 + \left(C_{FA}^{in}K_2Q_{Feed} - K_1^*\langle e^{a,S}(\underline{x})\rangle_{A_R}A_F - Q_{Feed}\right)^2}}{2K_2Q_{Feed}} \quad (28)$$

The experimental data were fitted again considering the simplified kinetic model (Eq. (28)), and the results of the kinetic parameters are shown in Table 4. Modeling and experimental FA outlet concentrations corresponding to different operating conditions are shown in Fig. 5. A satisfactory agreement is observed. Considering the whole set of operating conditions employed in this work, a root mean square error lower than 8.3% was obtained.

The effect of the inlet flow rate, inlet FA concentration, and irradiation level on the FA conversion is shown in Figs. 6–8, respectively. Experimental results have been included in these figures to support the tendencies of modeling results. Out of the total amount of performed experiments, in each of these figures, only those data where a single variable was separately modified are shown. Fig. 6 shows the experimental and modeling FA conversions obtained with different inlet flow rates, but keeping constant the remaining operating conditions (i.e., the irradiation level, the FA inlet concentration, and the recycle flow rate). FA conversion diminished when the inlet flow rate was increased as a consequence of the reduction of the residence time of reactants in the recycling system. Modeling results properly estimate experimental results. As expected, modeling FA conversion tends to 100% when the volumetric flow rate tends to zero. The dependence of the reactor conversion on the inlet FA concentration is shown in Fig. 7. Experimental and modeling results show that decreasing FA con-

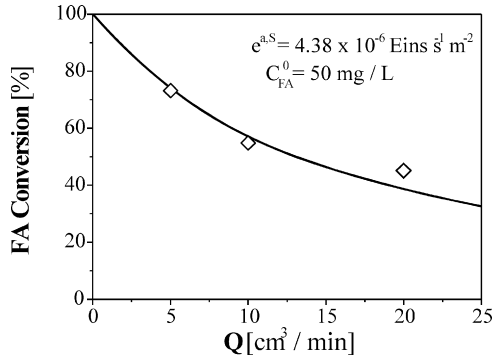

Fig. 6. FA conversion against the inlet flow rate: (◊) experimental measurements, (—) model simulations.

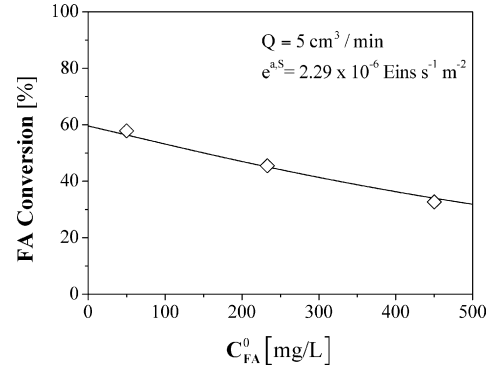

Fig. 7. FA conversion against the inlet FA concentration: (◊) experimental measurements, (—) model simulations.

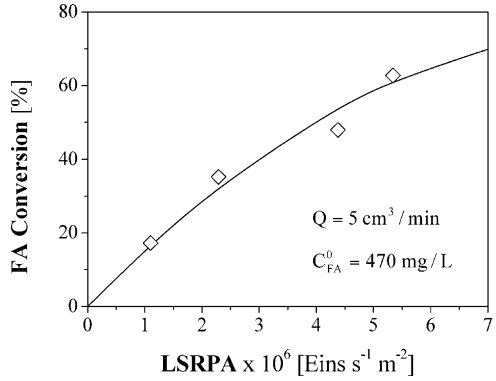

Fig. 8. FA conversion against the mean value of the LSRPA: (◊) experimental measurements, (—) model simulations.

versions were obtained when increasing concentrations were fed to the reactor recycle. Fig. 8 presents the modeling and experimental results of the FA conversions obtained with different irradiation levels. The efficiency of the reactor increased when the irradiation level of the reactor was augmented because the rate of generation of •OH radicals increases with the increment of the photon absorption rate.

7. Conclusions

A reactor–radiation–reaction kinetic model for a TiO_2-coated, quartz wool, packed-bed photocatalytic reactor aimed to degrade pollutants in water streams was developed. The reactor model was comprised of a reactor mass balance, a radiation model, and a kinetic model of the photocatalytic degradation of formic acid, which was used as the model pollutant. The local surface photon absorption rate (LSRPA) was obtained from a radiation model, which was solved using the Monte Carlo approach. The radiation model considers the interaction between photons and the TiO_2-coated fibers of the reactor. Based on a plausible reaction scheme, a kinetic model was proposed, whose parameters were estimated applying a nonlinear regression procedure using the experimental results obtained in a packed-bed reactor, operating in differential mode, and without mass transfer limitations. A satisfactory agreement was observed between model and experimental results, with a root mean square error lower than 8.3%

Acknowledgments

The authors are grateful to Universidad Nacional del Litoral (UNL), Consejo Nacional de Investigaciones Científicas y Técnicas (CONICET) and Agencia Nacional de Promoción Científica y Tecnológica (ANPCyT) for their financial support. This research was also supported by a grant to INCA "Consorzio Interuniversitario La Chimica per l'Ambiente" on Legge 488 funds, Research Project 3: "Rimozione di inquinanti mediante processi a membrana e fotocatalitici". Thanks are due also to Ing. Salvatore Castellana for the invaluable help in performing part of the experimental work.

Appendix I.

The local concentration of $[h^+]$ can be obtained from the local balance of electrons and holes:

$$[h^+] = \frac{k_2[O_2]_{ads}}{2k_{10}}\left(\sqrt{1+\frac{4k_{10}}{k_1k_2[H_2O]_{ads}[O_2]_{ads}}r_g}-1\right) \quad (A\text{-}1)$$

Similarly, the following expression can be obtained from the local balance of •OH radicals:

$$[\cdot OH] = \frac{k_1[H_2O]_{ads}}{k_3[FA]_{ads}+k_s}[h^+] \quad (A\text{-}2)$$

where k_s is the kinetic constant corresponding to the scavenging effect of •OH radicals produced by reactions (6), (7) and (A-2). Therefore, k_s is defined as:

$$k_s = k_6[H^+] + k_7[HO^-] + k_9[H_2O_2]_{ads} \quad (A\text{-}3)$$

In agreement with assumption (3), the FA degradation rate can be expressed as:

$$r_{FA} = -k_3[\cdot OH][FA] \quad (A\text{-}4)$$

Replacing Eqs. (A-1) and (A-2) into Eq. (A-4):

$$r_{FA} = -\frac{k_1k_2k_3}{2k_{10}}[H_2O]_{ads}[O_2]_{ads}\frac{[FA]_{ads}}{k_3[FA]_{ads}+k_s} \times\left(\sqrt{1+\frac{4k_{10}}{k_1k_2[H_2O]_{ads}[O_2]_{ads}}r_g}-1\right) \quad (A\text{-}5)$$

Since there were no mass transfer limitations, the surface concentration of adsorbed FA can be obtained from a balance of active sites. Consequently, surface concentrations can be related to bulk concentrations by means of the Langmuir isotherm:

$$[FA]_{ads} = \frac{K_{FA}[sites][FA]_{water}}{(1+K_{FA}[FA]_{water})} = \frac{K_{FA}[sites]C_{FA}}{(1+K_{FA}C_{FA})} \quad (A\text{-}6)$$

where K_{FA} is the adsorption equilibrium constant of FA and [sites] is the surface concentration of available sites for FA adsorption on

the TiO_2 catalyst film. Substituting Eq. (A-6) into Eq. (A-5):

$$r_{FA} = -\frac{k_1 k_2 k_3 [H_2O]_{ads} [O_2]_{ads} K_{FA} [sites] C_{FA}}{2k_{10}(k_s + (k_s + k_3[sites]) K_{FA} C_{FA})} \times \left(\sqrt{1 + \frac{4k_{10}}{k_1 k_2 [H_2O]_{ads} [O_2]_{ads}} r_g} - 1 \right) \quad \text{(A-8)}$$

The local surface rate of electron–hole pair generation, r_g, is given by:

$$r_g = \sum_{\lambda_{min}}^{\lambda_{max}} \Phi_\lambda e_\lambda^{a,S} \quad \text{(A-9)}$$

where Φ_λ is the spectral primary quantum yield for electron–hole generation at the catalytic surface. In the absence of information about the monochromatic quantum yield, Φ_λ, and resorting to the definition of a wavelength averaged primary quantum yield, $\langle \Phi \rangle$, Eq. (A-9) can be written:

$$r_g = \sum_{\lambda} \Phi_\lambda e_\lambda^{a,S} \cong \langle \Phi \rangle e^{a,S} \quad \text{(A-10)}$$

Substituting Eq. (A-10) into Eq. (A-8):

$$r_{FA} = -\frac{k_1 k_2 k_3 [H_2O]_{ads} [O_2]_{ads} K_{FA} [sites] C_{FA}}{2k_{10}(k_s + (k_s + k_3[sites]) K_{FA} C_{FA})} \times \left(\sqrt{1 + \frac{4k_{10} \langle \Phi \rangle}{k_1 k_2 [H_2O]_{ads} [O_2]_{ads}} e^{a,S}} - 1 \right) \quad \text{(A-11)}$$

Defining the following parameters:

$$K_1 = \frac{k_1 k_2 k_3 K_{FA}}{2k_{10} k_s} [H_2O]_{ads} [O_2]_{ads} [sites] \quad \text{(A-12)}$$

$$K_2 = \left(1 + \frac{k_3}{k_s} [sites]\right) K_{FA} \quad \text{(A-13)}$$

$$K_3 = \frac{4k_{10}}{k_1 k_2 [H_2O]_{ads} [O_2]_{ads}} \langle \Phi \rangle \quad \text{(A-14)}$$

and substituting Eqs. (A-12)–(A-14) into Eq. (A-11):

$$r_{FA} = -\frac{K_1 C_{FA}}{1 + K_2 C_{FA}} \left(\sqrt{1 + K_3 e^{a,S}} - 1 \right) \quad \text{(A-15)}$$

References

[1] G.E. Imoberdorf, G. Vella, A. Sclafani, L. Rizzuti, O.M. Alfano, A.E. Cassano, AIChE J. 56 (2010) 1030–1044.
[2] H. Al-Ekabi, N. Serpone, J. Phys. Chem. 92 (1988) 5726–5731.
[3] A. Sclafani, A. Brucato, L. Rizzuti, in: D.F. Ollis, H. Al-Ekabi (Eds.), Photocatalytic Purification and Treatment of Water and Air, Elsevier Science Publishers BV, Amsterdam, The Netherlands, 1993, pp. 533–545.
[4] J.C. Crittenden, R.P.S. Suri, D.L. Perram, D.W. Hand, Water Res. 31 (1997) 411–418.
[5] R. Changrani, G.B. Raupp, AIChE J. 45 (1999) 1085–1094.
[6] R. Changrani, G.B. Raupp, AIChE J. 46 (2000) 829–842.
[7] A.V. Vorontsov, E.E. Savinov, P.G. Smirniotis, Chem. Eng. Sci. 55 (2000) 5089–5098.
[8] D.D. Dionysiou, A.A. Burbano, M.T. Suidan, I. Baudin, J.-M. Laîné, Environ. Sci. Technol. 36 (2002) 3834–3843.
[9] A.O. Ibhadon, I.M. Arabatzis, P. Falaras, D. Tsoukleris, Chem. Eng. J. 133 (2007) 317–323.
[10] G. Spadoni, E. Bandini, F. Santarelli, Chem. Eng. Sci. 33 (1978) 517–524.
[11] T. Yokota, Y. Takahata, H. Nanjo, K. Takahashi, J. Chem. Eng. Jpn. 22 (1989) 537–542.
[12] M. Pasquali, F. Santarelli, J.F. Porter, P.L. Yue, AIChE J. 42 (1996) 532–536.
[13] T. Yokota, S. Cesur, H. Suzuki, H. Baba, Y. Takahata, J. Chem. Eng. Jpn. 32 (1999) 314–321.
[14] Q. Yang, P. Ling Ang, M.B. Ray, S.O. Pehkonen, Chem. Eng. Sci. 60 (2005) 5255–5268.
[15] G.E. Imoberdorf, O.M. Alfano, A.E. Cassano, H.A. Irazoqui, AIChE J. 53 (2007) 2688–2703.
[16] A. Brucato, A.E. Cassano, F. Grisafi, G. Montante, L. Rizzuti, G. Vella, AIChE J. 52 (2006) 3882–3890.
[17] A. Brucato, F. Grisafi, L. Rizzuti, A. Sclafani, G. Vella, Ind. Eng. Chem. Res. 46 (2007) 7684–7690.
[18] A. Alexiadis, Chem. Eng. Sci. 61 (2006) 516–525.
[19] M. Singh, I. Salvadó-Estivill, G. Li, Puma, AIChE J. 53 (2007) 678–686.
[20] D.H. Kim, M.A. Anderson, J. Photochem. Photobiol. A 94 (1996) 221–229.
[21] J.M. Kesselman, O. Weres, N.S. Lewis, M.R. Hoffmann, J. Phys. Chem. B 101 (1997) 2637–2643.
[22] R.J. Candal, W.A. Zeltner, M.A. Anderson, Environ. Sci. Technol. 34 (2000) 3443–3451.
[23] M.F.J. Dijkstra, H.J. Panneman, J.G.M. Winkelman, J.J. Kelly, A.A.C.M. Beenackers, Chem. Eng. Sci. 57 (2002) 4895–4907.
[24] T.A. McMurray, J.A. Byrne, P.S.M. Dunlop, J.G.M. Winkelman, B.R. Eggins, E.T. McAdams, Appl. Catal. A 262 (2004) 105–110.
[25] J. Krýsa, G. Waldner, H. Mesetankova, J. Jirkovsky, G. Grabner, Appl. Catal. B 64 (2006) 290–301.
[26] M. Mrowetz, E. Selli, J. Photochem. Photobiol. A 180 (2006) 15–22.
[27] G. Facchin, G. Carturan, R. Campostrini, S. Gialanella, L. Lutterotti, L. Armelao, G. Marcì, L. Palmisano, A. Sclafani, J. Sol–Gel Sci. Technol. 18 (2000) 29–59.
[28] G.E. Imoberdorf, H.A. Irazoqui, A.E. Cassano, O.M. Alfano, Ind. Eng. Chem. Res. 44 (16) (2005) 6643–6649.
[29] K. Wolf, D. Bockelmann, D. Bahnemann, in: B. Levt (Ed.), Proceeding of the IS&T 44th Annual Conference, IS&T, Springfiel, VA, 1991, pp. 259–267.
[30] D. Bahnemann, M. Hilgendorff, R. Memming, J. Phys. Chem. 101 (1997) 4265–4275.
[31] M.G. Gonzalez, E. Oliveros, M. Woerner, A.M. Braun, J. Photochem. Photobiol. C 5 (2004) 225–246.
[32] A.E. Cassano, C.A. Martín, R.J. Brandi, O.M. Alfano, Ind. Eng. Chem. Res. 34 (1995) 2155–2201.
[33] R. Siegel, J.R. Howell (Eds.), Thermal Radiation Heat Transfer, fourth ed., Hemisphere Publishing Corp, Bristol, PA, 2002.
[34] S. Sodergren, A. Hagfeldt, J. Olsson, S.E. Lindquist, J. Phys. Chem. 98 (1994) 5552–5556.
[35] O.M. Alfano, M.I. Cabrera, A.E. Cassano, J. Catal. 172 (1997) 370–379.